# Strain-sensitive superconductivity in the kagome metals $KV_3Sb_5$ and $CsV_3Sb_5$ probed by point-contact spectroscopy

Lichang Yin,[1,2,*] Dongting Zhang,[1,2,*] Chufan Chen,[1,2] Ge Ye,[1,2] Fanghang Yu,[3] Brenden R. Ortiz,[4] Shuaishuai Luo,[1,2] Weiyin Duan,[1,2] Hang Su,[1,2] Jianjun Ying,[3] Stephen D. Wilson,[4] Xianhui Chen,[3,5,6] Huiqiu Yuan,[1,2,6,7] Yu Song,[1,2,†] and Xin Lu[1,2,6,‡]

[1]*Center for Correlated Matter and Department of Physics, Zhejiang University, Hangzhou 310058, China*
[2]*Zhejiang Province Key Laboratory of Quantum Technology and Device, Department of Physics, Zhejiang University, Hangzhou 310058, China*
[3]*Hefei National Laboratory for Physical Sciences at Microscale and Department of Physics, and CAS Key Laboratory of Strongly-coupled Quantum Matter Physics, University of Science and Technology of China, Hefei, Anhui 230026, China*
[4]*Materials Department and California Nanosystems Institute, University of California Santa Barbara, Santa Barbara, California 93106, USA*
[5]*CAS Center for Excellence in Quantum Information and Quantum Physics, Hefei, Anhui 230026, China*
[6]*Collaborative Innovation Center of Advanced Microstructures, Nanjing 210093, China*
[7]*State Key Laboratory of Silicon Materials, Zhejiang University, Hangzhou 310058, China*

(Received 25 June 2021; revised 20 September 2021; accepted 26 October 2021; published 9 November 2021)

The kagome lattice is host to flat bands, topological electronic structures, Van Hove singularities, and diverse electronic instabilities, providing an ideal platform for realizing highly tunable electronic states. Here, we report soft and mechanical point-contact spectroscopy (SPCS and MPCS) studies of the kagome superconductors $KV_3Sb_5$ and $CsV_3Sb_5$. Compared to the superconducting transition temperature $T_c$ from specific heat and electrical resistance measurements, significantly enhanced values of $T_c$ are observed via the zero-bias conductance of SPCS, which become further enhanced in MPCS measurements. While the differential conductance curves from SPCS can be described by a two-gap *s*-wave model, a single *s*-wave gap reasonably captures the MPCS data, likely due to a diminishing spectral weight of the other gap. The enhanced superconductivity probably arises from local strain caused by the point contact, which also leads to two-gap or single-gap behaviors observed in different point contacts. Our results demonstrate highly strain-sensitive superconductivity in kagome metals $CsV_3Sb_5$ and $KV_3Sb_5$, which may be harnessed in the manipulation of possible Majorana zero modes.

DOI: 10.1103/PhysRevB.104.174507

## I. INTRODUCTION

Due to its unique geometry, the kagome lattice natively hosts electronic flat bands, Dirac band crossings, and Van Hove singularities, allowing for the realization of distinct topological electronic states [1–4] and correlated collective orders [5–10]. The recent discovery of superconductivity in the kagome metals $AV_3Sb_5$ ($A$ = K, Rb, Cs) [11–14] triggered immense interest, as superconductivity in these materials coexists with topologically protected surface states [12] and an unusual chiral charge order [15,16], offering an ideal platform to investigate the interplay between these exotic phenomena and their evolution upon tuning.

While the nature of the superconducting pairing in $AV_3Sb_5$ is still under debate [17–21], signatures of spin-triplet supercurrents were found in $K_{1-x}V_3Sb_5$ Josephson junctions [22], and possible Majorana zero modes have been detected in $CsV_3Sb_5$ [23]. These findings raise the possibility that $AV_3Sb_5$ may exhibit topological superconductivity with potential applications in fault-tolerant quantum computation [24–26]. Superconductivity in $AV_3Sb_5$ is highly susceptible to pressure, displaying two superconducting domes in the temperature-pressure phase diagram [17,27–31], and a roughly triple enhancement of the superconducting transition temperature $T_c$ can be realized under modest pressures of ≈1 GPa. The tunability of superconductivity under pressure suggests that it may be modulated by strain, for example to induce superconductor-metal transitions or to stabilize superconductor-metal heterostructures, and raises prospects for the strain-manipulation of possible Majorana zero modes.

In this work, we applied soft and mechanical point-contact spectroscopy (SPCS and MPCS) to investigate the superconducting properties of single crystalline $CsV_3Sb_5$ and $KV_3Sb_5$. From both temperature and field dependence of the zero-bias conductance, as well as analyses of the differential conductance curves $G(V)$ with the Blonder-Tinkham-Klapwijk (BTK) model, we observed that values of $T_c$ in SPCS and MPCS are substantially enhanced relative to those from thermodynamic and transport measurements. The enhancement of superconductivity is attributed to local strain in the point-contact region, consistent with the larger enhancement observed in MPCS. While describing the differential conductance from SPCS requires two *s*-wave gaps, a single gap

*These authors contributed equally to this work.
†Corresponding author: yusong_phys@zju.edu.cn
‡Corresponding author: xinluphy@zju.edu.cn

 

is sufficient to capture the MPCS results. Nonetheless, the anomalously small ratio between the superconducting gap and $T_c$ in the MPCS results suggests the presence of an undetected larger gap. Our results demonstrate highly strain-sensitive superconductivity in the kagome metals $KV_3Sb_5$ and $CsV_3Sb_5$, and are consistent with nodeless multigap pairing.

## II. EXPERIMENTAL DETAILS

High quality single crystals of $CsV_3Sb_5$ and $KV_3Sb_5$ were synthesized using the self-flux method [12,13]. SPCS measurements were performed by attaching a gold wire (30 $\mu$m in diameter) onto cleaved samples through a drop of silver paint, forming hundreds of parallel nanoscale conducting channels between individual silver particles and the sample surface. The contact areas have diameters in the range 50–100 $\mu$m. Electrical resistance measurements were carried out on the same samples with four-probes. MPCS measurements were carried out in an anvil-needle configuration, where electrochemically etched gold tips are employed and piezo-controlled nanopositioners are used to gently control the engagement between the tip and the sample. Differential conductance as a function of the bias voltage $G(V)$ was recorded with the lock-in technique in a quasi-four-probe configuration. An Oxford Instruments cryostat with a $^3$He insert (base temperature 0.3 K) was used for SPCS and MPCS measurements, and magnetic fields up to 3.5 T were applied along the $c$ axis. Point-contact areas in both SPCS and MPCS measurements are in the $ab$ plane.

## III. RESULTS

### A. Zero-bias conductance

For a superconductor, an increase in conductance under zero bias signals the appearance of Andreev reflection, and serves as a proxy for the onset of superconductivity. Whereas specific heat mostly probes bulk superconductivity, and resistance is, in addition, sensitive to superconducting filaments or patches, the zero-bias conductance is dominated by superconductivity in the point-contact area.

In Figs. 1(a)–1(c), the zero-bias conductance $G(V = 0)$ of $CsV_3Sb_5$ from SPCS and MPCS measurements are compared with electrical resistance measured on the same samples used for SPCS, and electronic specific heat $C_e(T)/\gamma T$ was measured previously on samples from the same batch [18,28]. In contrast to superconductivity that onsets below $T_c \approx 2.8$ K in $C_e(T)/\gamma T$, the temperature dependence of $G(V = 0)$ for $CsV_3Sb_5$ indicates an onset of Andreev reflection below $\approx$4.2 K for SPCS and $\approx$5.0 K for MPCS, suggesting the $T_c$ probed by point-contact spectroscopy is significantly enhanced. Similar behaviors are observed in $KV_3Sb_5$, with a $T_c \approx 1.0$ K in $C_e(T)/\gamma T$ increased to $\approx$1.8 K for SPCS and $\approx$3.1 K for MPCS, as shown in Figs. 1(e)–1(g). Signatures of superconductivity from Andreev reflection [Figs. 1(a) and 1(e)] also appear at higher temperatures compared to resistance [Figs. 1(b) and 1(f)], and with a higher onset temperature in MPCS than SPCS for both $CsV_3Sb_5$ and $KV_3Sb_5$. These observations unequivocally point to enhanced superconductivity in SPCS and MPCS measurements, compared to both specific heat and electrical transport measurements.

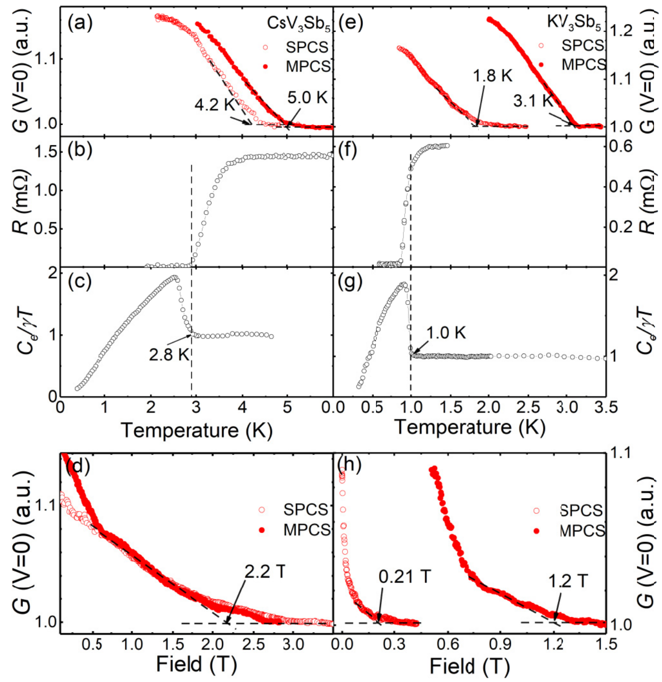


FIG. 1. Temperature dependence of the zero-bias conductance $G(V = 0)$ measured using SPCS and MPCS for (a) $CsV_3Sb_5$ and (e) $KV_3Sb_5$. Electrical resistance $R(T)$ was carried out on the same samples, as shown in (b) for $CsV_3Sb_5$, and (f) for $KV_3Sb_5$. $C_e(T)/\gamma T$ data for (c) $CsV_3Sb_5$ and (g) $KV_3Sb_5$, respectively from Refs. [18] and [28]. Field dependence of the zero-bias conductance $G(V = 0)$ measured using SPCS and MPCS at $T = 0.3$ K for (d) $CsV_3Sb_5$ and (h) $KV_3Sb_5$, with the field along the $c$ axis.

Given that enhanced superconductivity is not observed in scanning tunneling microscopy measurements [23,32], the increase of $T_c$ from Andreev reflection in Figs. 1(a) and 1(e) likely results from effects of point contacts on the sample, rather than associated with the sample surface. Since superconductivity in $AV_3Sb_5$ is highly responsive to pressure [17,27–31], local strain induced by point contacts may be responsible for the enhanced superconductivity. The observation of a larger tuning effect in MPCS relative to SPCS is consistent with this scenario, since mechanical point contacts typically lead to a larger strain compared to soft point contacts. The enhanced superconductivity also manifests through increased upper critical fields $H_{c2}$ at $T = 0.3$ K ($H \parallel c$): it is $\approx$0.21 T for SPCS and $\approx$1.2 T for MPCS measurements on $KV_3Sb_5$ [Fig. 1(h)]. In $CsV_3Sb_5$, we find $H_{c2} \approx$ 2.2 T ($H \parallel c$) for both SPCS and MPCS [Fig. 1(d)], significantly higher than $H_{c2} \approx 1.0$ T determined from resistivity measurements [33].

### B. Differential conductance curves from SPCS

To probe the superconducting state with enhanced $T_c$, we systematically measured the differential conductance curves $G(V)$ for $CsV_3Sb_5$ and $KV_3Sb_5$ at various temperatures and under different magnetic fields, with SPCS results in Figs. 2–4, and MPCS results in Figs. 5 and 6. A representative set of SPCS $G(V)$ curves at 0.3 K for $CsV_3Sb_5$ are shown in Figs. 2(a)–2(c), while those for $KV_3Sb_5$ are shown in

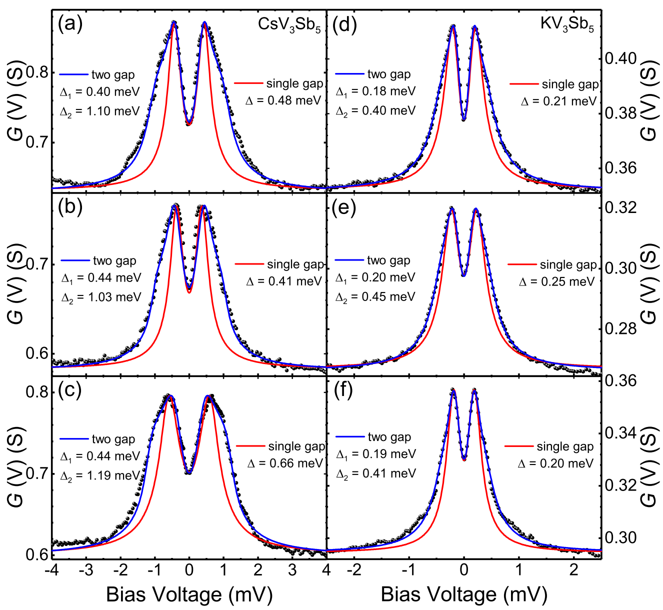


FIG. 2. Representative SPCS differential conductance curves for (a)–(c) $CsV_3Sb_5$ and (d)–(f) $KV_3Sb_5$ at $T = 0.3$ K. Solid red lines are fits to a single-gap $s$-wave model for data with voltages below the peak in $G(V)$. The solid blue lines are fits to a two-gap $s$-wave model. The slight deviation of the measured differential conductance from the fits at large bias voltages is due to current heating effects [34].

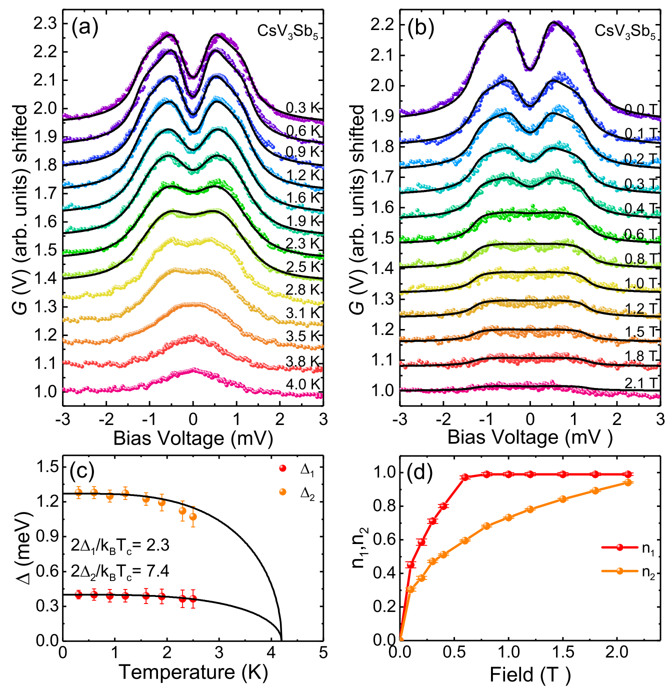


FIG. 3. Normalized differential conductance curves for $CsV_3Sb_5$ from SPCS, as a function of (a) temperature and (b) magnetic field. The solid lines are fits to the two-gap $s$-wave BTK models at finite temperatures or under applied magnetic fields. The extracted superconducting gaps $\Delta_1$ and $\Delta_2$ are shown in (c) as a function of temperature with $H = 0$ T and the solid lines are based on the BCS theory with $T_c$ estimated from the zero-bias conductance. The extracted fraction of normal state vortex core excitations $n_1$ and $n_2$ are shown in (d) as a function of magnetic field at $T = 0.3$ K.

Figs. 2(d)–2(f). All the conductance curves for $CsV_3Sb_5$ show a double-peak feature around 0.5 mV and a small bulge around 1 mV, characteristic of two-gap superconductivity. A single-gap $s$-wave BTK model fails to describe the $G(V)$ curves, with substantial deviations of the fits from the experimental data. On the other hand, a two-band BTK model, $G(V) \propto \omega G_1(V) + (1-\omega)G_2(V)$ $(0 \leqslant \omega \leqslant 1)$, with a small ($\Delta_1 \sim 0.4$ meV) and a large gap ($\Delta_2 \sim 1.1$ meV) captures the experimental data, shown as solid blue lines in Figs. 2(a)–2(c). $\omega$ ranges 60–80%, indicating that the small gap exhibits a dominant spectral weight. Similarly, we find that the differential conductance $G(V)$ curves for $KV_3Sb_5$ from SPCS [solid red lines in Figs. 2(d)–2(f)] cannot be satisfactorily captured by a single-gap $s$-wave model. On the other hand, the data can be consistently described by a two-gap $s$-wave model with $\Delta_1 \sim 0.18$ meV and $\Delta_2 \sim 0.38$ meV, with $\omega$ in the range 20–70%. Our results suggest that despite enhanced gap values induced by local strain in our SPCS measurements, the superconducting gap structures in both $CsV_3Sb_5$ and $KV_3Sb_5$ can be appropriately described by a two-gap $s$-wave model, consistent with nodeless multigap superconductivity in unstrained $CsV_3Sb_5$ revealed through magnetic penetration depth and specific heat measurements [18].

Temperature evolution of the differential conductance $G(V)$ curves for SPCS on $CsV_3Sb_5$ is shown in Fig. 3(a). With increasing temperature, the double peaks gradually shift towards the center, merging into a single zero-bias peak that disappears as temperature approaches $T_c$. To extract the temperature dependence of the superconducting gaps $\Delta_1$ and $\Delta_2$, we fit the $G(V)$ curves to the two-gap $s$-wave BTK model with $\omega$ constrained to its value at 0.3 K ($\omega = 0.674$), shown as solid lines in Fig. 3(a). While the two-gap model is clearly better than the single-gap model in describing $G(V)$ curves at low temperatures (Fig. 2), for $T \gtrsim 2.5$ K both models can reasonably capture the data. In such a situation, although a two-gap behavior is expected to persist, it is no longer possible to reliably and independently determine $\Delta_1$ and $\Delta_2$. The extracted values of $\Delta_1$ and $\Delta_2$ from fits in Fig. 3(a) are shown in Fig. 3(c), and the solid black lines are the expected behavior from BCS theory, with $T_c = 4.2$ K inferred from the zero-bias conductance in Fig. 1(a). The superconducting gaps at zero temperature are found to be $\Delta_1 = 0.4$ meV and $\Delta_2 = 1.27$ meV, yielding $2\Delta_1/k_BT_c = 2.3$ and $2\Delta_2/k_BT_c = 7.4$. The larger gap clearly exceeds $2\Delta/k_BT_c = 3.52$ in the weak-coupling limit, while the smaller gap is well below it. Such a behavior is characteristic of two-gap superconductors such as $MgB_2$ [35].

The magnetic field dependence of $G(V)$ for SPCS on $CsV_3Sb_5$ at 0.3 K is shown in Fig. 3(b), with the field along the $c$ axis. For a superconductor with vortices, its point-contact conductance contains contributions from both the normal and superconducting states. In the case of a two-gap superconductor, the normalized point-contact conductance can be modeled using a modified two-gap BTK model, with $G(V) \propto \omega[n_1 + (1-n_1)G_1(V)] + (1-\omega)[n_2 + (1-n_2)G_2(V)]$, where $n_1$ and $n_2$ correspond to the fractions of the normal-state vortex core excitations [36,37]. Fits to this model are shown as solid lines in Fig. 3(b), with all parameters

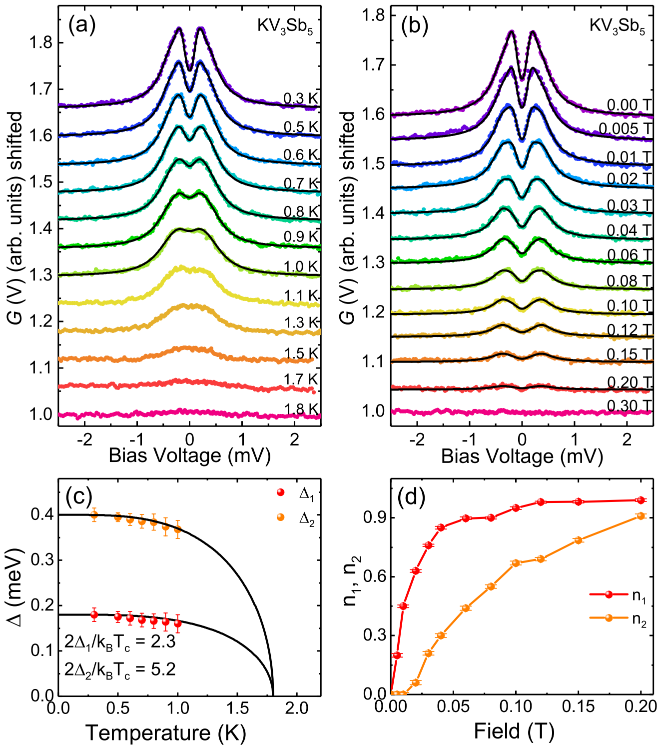

FIG. 4. Normalized differential conductance curves for $KV_3Sb_5$ from SPCS, as a function of (a) temperature and (b) magnetic field. The solid lines are fits to the two-gap *s*-wave BTK model at finite temperatures or under applied magnetic fields. The extracted superconducting gaps $\Delta_1$ and $\Delta_2$ are shown in (c) as a function of temperature with $H = 0$ T and the solid lines are based on the BCS theory with $T_c$ estimated from the zero-bias conductance. The extracted fraction of normal state vortex core excitations $n_1$ and $n_2$ is shown in (d) as a function of magnetic field at $T = 0.3$ K.

aside from $n_1$ and $n_2$ fixed to those from BTK fits under zero field and at $T = 0.3$ K. The extracted values of $n_1$ and $n_2$ are shown in Fig. 3(d), as a function of magnetic field. With increasing field, $n_1$ saturates before $n_2$, indicating that $\Delta_1$ is more sensitive to applied fields. Overall, the qualitative evolution of $n_1$ and $n_2$ with applied magnetic field resembles behaviors in $MgB_2$ [36,37].

Similar SPCS measurements were carried out for $KV_3Sb_5$, with results shown in Fig. 4. The differential conductance curves at different temperatures show that they flatten above $\approx$1.8 K [Fig. 4(a)], significantly above $T_c = 1.0$ K from specific heat. For $KV_3Sb_5$, the values of $\Delta_1$ and $\Delta_2$ can be reliably extracted for $T \leqslant 1.0$ K ($H = 0$ T), with values shown in Fig. 4(c). The temperature evolution of the two gaps are consistent with expectations of the BCS theory, with $T_c = 1.8$ K determined from the zero-bias conductance [Fig. 1(e)]. From the extracted gap values, we find $2\Delta_1/k_BT_c = 2.3$ and $2\Delta_2/k_BT_c = 5.2$, similar to $CsV_3Sb_5$. From measurements under applied fields [Fig. 4(b)], $n_1$ is found to saturate before $n_2$ [Fig. 4(d)], similar to $CsV_3Sb_5$.

### C. Differential conductance curves from MPCS

In order to have a comparative study of how strain affects the superconducting state of $AV_3Sb_5$, we applied MPCS

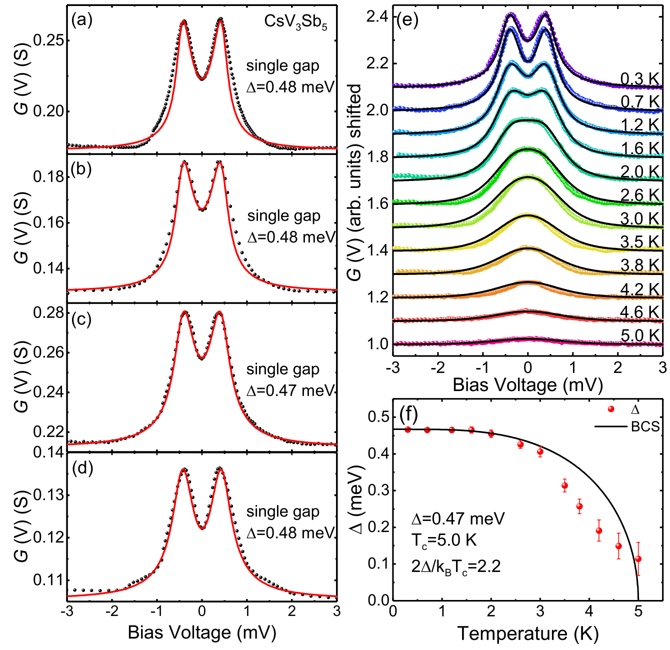

FIG. 5. (a)–(d) Representative MPCS differential conductance curves for $CsV_3Sb_5$ at $T = 0.3$ K. The red solid line are fits to a single-gap *s*-wave BTK model. (e) Temperature evolution of the MPCS differential conductance curves for $CsV_3Sb_5$, fit to a single-gap *s*-wave BTK model (black solid lines). (f) Temperature dependence of the extracted superconducting gap $\Delta$ from (e); the black line is the expected behavior of the BCS theory, with $\Delta = 0.47$ meV and $T_c = 5.0$ K ($2\Delta/k_B\mathrm{T}_c = 2.2$).

to study both $CsV_3Sb_5$ and $KV_3Sb_5$, with results shown in Fig. 5 for $CsV_3Sb_5$ and Fig. 6 for $KV_3Sb_5$. In the case of $CsV_3Sb_3$, we find the measured differential conductance curves can be reasonably fit by a single-gap *s*-wave model [Figs. 6(a)–6(d)], with $\Delta \approx 0.47$ meV. However, from the zero-bias conductance [Fig. 1(a)] and temperature-dependent conductance curves [Fig. 5(e)], we find $T_c \approx 5.0$ K, which leads to $2\Delta/k_BT_c \approx 2.2$. This value is significantly smaller than the BCS weak-coupling limit of 3.52, but is similar to $2\Delta_1/k_BT_c \approx 2.3$ from SPCS measurements on $CsV_3Sb_5$.

By analyzing the differential conductance curves with the single-gap *s*-wave model, we find the temperature dependence of $\Delta$ clearly deviates from BCS theory [Fig. 5(f)]. In combination with the small values of $2\Delta/k_BT_c$, these behaviors are reminiscent of the proximity effect [38]. In such a scenario, the intrinsic $T_c$ of the point-contact area is low, and proximity to a system with higher $T_c$ enhances $T_c$ but not the gap value at low temperatures.

However, in the present case, the bulk $T_c$ of the sample (determined from specific heat and resistance measurements) is lower compared to what is measured by MPCS, which means that the point-contact area exhibits a higher $T_c$ and that the proximity effect is unlikely to be operative. Instead, a more plausible explanation for the small value of $2\Delta/k_BT_c$ is that there may be a larger gap in MPCS measurements, which is undetected due to a diminishing spectral weight. In this scenario, only the smaller gap is detected, and its anomalous temperature dependence resembles that of the smaller gap in some two-gap superconductors [39,40].

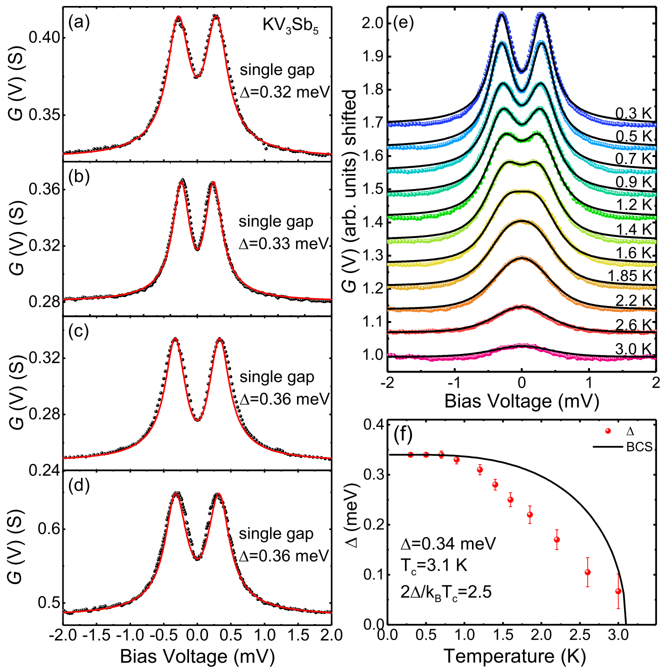


FIG. 6. (a)–(d) Representative MPCS differential conductance curves for $KV_3Sb_5$ at $T = 0.3$ K. The solid red lines are fits to a single-gap *s*-wave BTK model. (e) Temperature evolution of the MPCS differential conductance curves for $KV_3Sb_5$, fit to a single-gap *s*-wave BTK model (black solid lines). (f) Temperature dependence of the extracted superconducting gap Δ from (e); the black line is the expected behavior of the BCS theory, with $\Delta = 0.34$ meV and $T_c = 3.1$ K ($2\Delta/k_BT_c = 2.5$).

Similar behaviors are found for MPCS on $KV_3Sb_5$, as shown in Fig. 6. The differential conductance curves are also reasonably accounted for using a single-gap *s*-wave model, with $\Delta \approx 0.34$ meV [Figs. 6(a)–6(d)]. Combined with $T_c \approx 3.1$ K from Figs. 1(e) and 6(e), we obtain $2\Delta/k_BT_c \approx 2.5$, also significantly smaller than 3.52, and clear deviations of Δ from the BCS theory are also observed in its temperature evolution [Fig. 6(f)]. Our MPCS measurements suggest that $CsV_3Sb_5$ and $KV_3Sb_5$ are similar, and both likely exhibit multigap superconductivity, although the larger gap may be undetected in MPCS measurements likely due to a diminished spectral weight.

## IV. DISCUSSION AND CONCLUSION

The observations of an exponential temperature dependence of the magnetic penetration depth [18], a Hebel-Slichter coherence peak from nuclear magnetic resonance [19], and sensitivity of the superconducting state to magnetic impurities from scanning tunneling microscopy measurements [20] point to nodeless multigap superconductivity in $AV_3Sb_5$. On the other hand, a robust nodal superconducting state has been suggested by thermal conductivity measurements [17], and certain theoretical considerations [21].

All differential conductance curves in Figs. 2–6 from SPCS and MPCS can be consistently described by a two-gap *s*-wave model, although the larger gap in MPCS measurements has a diminishing spectral weight. Our results are therefore consistent with nodeless multigap superconductivity in the $AV_3Sb_5$ series, although $T_c$ observed in our measurements are strongly enhanced relative to unstrained samples. Nodeless multigap superconductivity derived from unstrained samples provides a natural explanation for the multigap phenomenology in our point-contact spectroscopy measurements. However, real space strain inhomogeneity may also contribute to the multigap phenomenology, especially in SPCS measurements where the point contacts are large (50–100 $\mu$m) and possible interactions between the silver paste and $AV_3Sb_5$ samples are not yet fully understood. Further work is needed to distinguish between reciprocal and real space contributions to the multigap behaviors observed in our point-contact spectroscopy measurements.

In point-contact spectroscopy measurements on layered materials, perfectly two-dimensional Fermi sheets do not contribute to the differential conductance for point contact areas in the *ab*-plane. As a Fermi surface becomes progressively more corrugated along the *c*-axis direction, its spectral weight in the differential conductance increases in tandem. Therefore, within the multigap pairing scenario, the differing spectral weight of the large and small superconducting gaps between SPCS and MPCS measurements may correspond to varying degrees of out-of-plane dispersion in the normal state electronic structures. In such a situation, the small spectral weight of the larger gap in MPCS measurements suggests that the larger strain in MPCS measurements leads to the corresponding band becoming more two-dimensional compared to SPCS measurements, and points to a nontrivial effect of strain on the normal state electronic structure of $AV_3Sb_5$.

For SPCS measurements, local stress or strain may arise during curing of the silver paste or upon cooling due to differential thermal contraction between the sample and the silver paste. As these effects are usually weak, they can be ignored in most SPCS measurements. However, given the tendency of $AV_3Sb_5$ crystals to exfoliate, lateral stress could be limited to a few layers near the surface, which can induce a sizable strain even if the stress is small. Such sizable strains coupled with the sensitivity to pressure (and thus strain) [17,27–31] likely account for the enhanced superconductivity observed in $CsV_3Sb_5$ and $KV_3Sb_5$ from our SPCS measurements.

In addition, as $AV_3Sb_5$ are good metals with a large density of states at the Fermi level, charge doping through the silver paste should play a minor role in enhancing superconductivity. In contrast, both strain effects and charge doping may be operative in the dramatic enhancement of $T_c$ seen in $MoTe_2$ from SPCS measurements [41], as $MoTe_2$ is a semimetal with superconductivity sensitive to pressure [42]. In addition, electron-phonon coupling may be important for the sensitivity of superconductivity to strain. This is because electron-phonon coupling is involved in both superconductivity and the charge order, and the competition between the two orders plays a key role in the enhancement of $T_c$ under pressure [28].

Compared to SPCS, a more significant strain is typically applied by the sharp tip in MPCS measurements, consistent with the more significant increase in $T_c$. It should be noted that whereas strain is dominantly in the *ab* plane for SPCS, it is mostly along the *c* axis for MPCS. The observation of enhanced $T_c$ in both approaches then indicates that superconductivity in $AV_3Sb_5$ is sensitive to strain in more than one symmetry channel, and motivates further studies on the evolution of superconductivity in $AV_3Sb_5$ under uniaxial strain. In addition, since the *c* axis collapses more readily under hydrostatic pressure [30,43], the large susceptibility of the crystal structure to *c*-axis stress may also contribute to the stronger effect of mechanical point contact on superconductivity. A dramatic increase in $T_c$ was also reported in FeSe through MPCS measurements [44], which is also a highly two-dimensional material with superconductivity that becomes enhanced under hydrostatic pressure [45,46]. Taking the results on $AV_3Sb_5$, $MoTe_2$, and FeSe together, it appears that layered materials with superconductivity that becomes enhanced under hydrostatic pressure are susceptible to strain effects in point-contact spectroscopy measurements.

Compared to hydrostatic pressure, strain is much easier to realize and manipulate in devices, giving it a unique advantage in practical applications. Our results demonstrate that local strain from point contacts are sufficient to dramatically tune the superconducting properties of $AV_3Sb_5$, and suggests that such strain-sensitive superconductivity may be useful in device engineering, for example, in realizing superconductor-metal heterostructures. Furthermore, strain may be utilized in the manipulation of possible Majorana zero modes in these materials [23].

The values of $2\Delta_2/k_B T_c$ from SPCS measurements are especially notable, as they are significantly larger than corresponding values from unstrained samples [18,23,32], and are difficult to understand even if possible real space inhomogeneities are taken into consideration. One possible origin for such large values is that strain in the SPCS measurements leads to enhanced electronic correlations in the point-contact area. However, understanding the origin for the large gaps observed with SPCS measurements requires further investigations.

In conclusion, we performed SPCS and MPCS measurements on $CsV_3Sb_5$ and $KV_3Sb_5$, and observed enhanced superconductivity in all cases. This enhancement likely originates from local strain induced by the point contacts, since similar enhancements are absent in scanning tunneling microscopy measurements. While the superconducting gap structure is better described by a two-gap *s*-wave model for SPCS results (as in $MgB_2$), a single-gap BTK model can reasonably capture the MPCS results, pointing to a nontrivial effect of strain tuning. Our findings highlight the sensitivity of superconductivity to strain in the kagome metals $AV_3Sb_5$, which may be useful in the device engineering of these materials.

## ACKNOWLEDGMENTS

We are grateful for valuable discussions with C. Cao and Y. Liu. The work at Zhejiang University was supported by the National Key R&D Program of China (Grants No. 2017YFA0303100 and No. 2016YFA0300202), the Key R&D Program of Zhejiang Province, China (Grant No. 2021C01002), the National Natural Science Foundation of China (Grants No. 12174333, No. 11974306, and No. 12034017), and the Fundamental Research Funds for the Central Universities of China. X.L. would like to acknowledge support from the Zhejiang Provincial Natural Science Foundation of China (Grant No. LR18A04001). S.D.W. and B.R.O. gratefully acknowledge support via the UC Santa Barbara NSF Quantum Foundry funded via the Q-AMASE-i program under Award No. DMR-1906325. B.R.O. also acknowledges support from the California NanoSystems Institute through the Elings fellowship program.

[1] L. Ye, M. Kang, J. Liu, F. von Cube, C. R. Wicker, T. Suzuki, C. Jozwiak, A. Bostwick, E. Rotenberg, D. C. Bell *et al.*, Nature (London) **555**, 638 (2018).

[2] E. Liu, Y. Sun, N. Kumar, L. Muechler, A. Sun, L. Jiao, S.-Y. Yang, D. Liu, A. Liang, Q. Xu *et al.*, Nat. Phys. **14**, 1125 (2018).

[3] M. Kang, L. Ye, S. Fang, J.-S. You, A. Levitan, M. Han, J. I. Facio, C. Jozwiak, A. Bostwick, E. Rotenberg *et al.*, Nat. Mater. **19**, 163 (2019).

[4] J.-X. Yin, W. Ma, T. A. Cochran, X. Xu, S. S. Zhang, H.-J. Tien, N. Shumiya, G. Cheng, K. Jiang, B. Lian *et al.*, Nature (London) **583**, 533 (2020).

[5] W.-S. Wang, Z.-Z. Li, Y.-Y. Xiang, and Q.-H. Wang, Phys. Rev. B **87**, 115135 (2013).

[6] S. V. Isakov, S. Wessel, R. G. Melko, K. Sengupta, and Y. B. Kim, Phys. Rev. Lett. **97**, 147202 (2006).

[7] H.-M. Guo and M. Franz, Phys. Rev. B **80**, 113102 (2009).

[8] M. L. Kiesel, C. Platt, and R. Thomale, Phys. Rev. Lett. **110**, 126405 (2013).

[9] J. Wen, A. Rüegg, C.-C. J. Wang, and G. A. Fiete, Phys. Rev. B **82**, 075125 (2010).

[10] T. Park, M. Ye, and L. Balents, Phys. Rev. B **104**, 035142 (2021).

[11] B. R. Ortiz, L. C. Gomes, J. R. Morey, M. Winiarski, M. Bordelon, J. S. Mangum, I. W. H. Oswald, J. A. Rodriguez-Rivera, J. R. Neilson, S. D. Wilson, E. Ertekin, T. M. McQueen, and E. S. Toberer, Phys. Rev. Mater. **3**, 094407 (2019).

[12] B. R. Ortiz, S. M. L. Teicher, Y. Hu, J. L. Zuo, P. M. Sarte, E. C. Schueller, A. M. Milinda Abeykoon, M. J. Krogstad, S. Rosenkranz, R. Osborn, R. Seshadri, L. Balents, J. He, and S. D. Wilson, Phys. Rev. Lett. **125**, 247002 (2020).

[13] B. R. Ortiz, P. M. Sarte, E. M. Kenney, M. J. Graf, S. M. L. Teicher, R. Seshadri, and S. D. Wilson, Phys. Rev. Mater. **5**, 034801 (2021).

[14] Q. Yin, Z. Tu, C. Gong, Y. Fu, S. Yan, and H. Lei, Chin. Phys. Lett. **38**, 037403 (2021).

[15] Y.-X. Jiang, J.-X. Yin, M. M. Denner, N. Shumiya, B. R. Ortiz, G. Xu, Z. Guguchia, J. He, M. S. Hossain, X. Liu *et al.*, Nat. Mater. **20**, 1353 (2021).

[16] X. Feng, K. Jiang, Z. Wang, and J. Hu, Sci. Bull. **66**, 1384 (2021).

[17] C. C. Zhao, L. S. Wang, W. Xia, Q. W. Yin, J. M. Ni, Y. Y. Huang, C. P. Tu, Z. C. Tao, Z. J. Tu, C. S. Gong *et al.*, arXiv:2102.08356.

[18] W. Duan, Z. Nie, S. Luo, F. Yu, B. R. Ortiz, L. Yin, H. Su, F. Du, A. Wang, Y. Chen *et al.*, Sci. China-Phys. Mech. Astron. **64**, 107462 (2021).

[19] C. Mu, Q. Yin, Z. Tu, C. Gong, H. Lei, Z. Li, and J. Luo, Chin. Phys. Lett. **38**, 077402 (2021).

[20] H.-S. Xu, Y.-J. Yan, R. Yin, W. Xia, S. Fang, Z. Chen, Y. Li, W. Yang, Y. Guo, and D.-L. Feng, Phys. Rev. Lett. **127**, 187004 (2021).

[21] X. Wu, T. Schwemmer, T. Müller, A. Consiglio, G. Sangiovanni, D. D. Sante, Y. Iqbal, W. Hanke, A. P. Schnyder, M. M. Denner *et al.*, Phys. Rev. Lett. **127**, 177001 (2021).

[22] Y. Wang, S. Yang, P. K. Sivakumar, B. R. Ortiz, S. M. L. Teicher, H. Wu, A. K. Srivastava, C. Garg, D. Liu, S. S. P. Parkin *et al.*, arXiv:2012.05898.

[23] Z. Liang, X. Hou, F. Zhang, W. Ma, P. Wu, Z. Zhang, F. Yu, J.-J. Ying, K. Jiang, L. Shan, Z. Wang, and X.-H. Chen, Phys. Rev. X **11**, 031026 (2021).

[24] S. D. Sarma, M. Freedman, and C. Nayak, npj Quantum Inf. **1**, 15001 (2015).

[25] Y. Tanaka, M. Sato, and N. Nagaosa, J. Phys. Soc. Jpn. **81**, 011013 (2012).

[26] M. Sato and Y. Ando, Rep. Prog. Phys. **80**, 076501 (2017).

[27] K. Y. Chen, N. N. Wang, Q. W. Yin, Y. H. Gu, K. Jiang, Z. J. Tu, C. S. Gong, Y. Uwatoko, J. P. Sun, H. C. Lei, J. P. Hu, and J. G. Cheng, Phys. Rev. Lett. **126**, 247001 (2021).

[28] F. Du, S. Luo, B. R. Ortiz, Y. Chen, W. Duan, D. Zhang, X. Lu, S. D. Wilson, Y. Song, and H. Yuan, Phys. Rev. B **103**, L220504 (2021).

[29] F. Yu, D. Ma, W. Zhuo, S. Liu, X. Wen, B. Lei, J. Ying, and X. Chen, Nat. Commun. **12**, 3645 (2021).

[30] Z. Zhang, Z. Chen, Y. Zhou, Y. Yuan, S. Wang, J. Wang, H. Yang, C. An, L. Zhang, X. Zhu, Y. Zhou, X. Chen, J. Zhou, and Z. Yang, Phys. Rev. B **103**, 224513 (2021).

[31] C. C. Zhu, X. F. Yang, W. Xia, Q. W. Yin, L. S. Wang, C. C. Zhao, D. Z. Dai, C. P. Tu, B. Q. Song, Z. C. Tao *et al.*, arXiv:2104.14487.

[32] H. Chen, H. Yang, B. Hu, Z. Zhao, J. Yuan, Y. Xing, G. Qian, Z. Huang, G. Li, Y. Ye *et al.*, Nature (2021), doi:10.1038/s41586-021-03983-5.

[33] S. Ni, S. Ma, Y. Zhang, J. Yuan, H. Yang, Z. Lu, N. Wang, J. Sun, Z. Zhao, D. Li *et al.*, Chin. Phys. Lett. **38**, 057403 (2021).

[34] G. Sheet, S. Mukhopadhyay, and P. Raychaudhuri, Phys. Rev. B **69**, 134507 (2004).

[35] A. Brinkman, A. A. Golubov, H. Rogalla, O. V. Dolgov, J. Kortus, Y. Kong, O. Jepsen, and O. K. Andersen, Phys. Rev. B **65**, 180517(R) (2002).

[36] Y. Bugoslavsky, Y. Miyoshi, G. K. Perkins, A. D. Caplin, L. F. Cohen, A. V. Pogrebnyakov, and X. X. Xi, Phys. Rev. B **72**, 224506 (2005).

[37] P. Szabó, P. Samuely, Z. Pribulová, M. Angst, S. Bud'ko, P. C. Canfield, and J. Marcus, Phys. Rev. B **75**, 144507 (2007).

[38] A. Gilabert, J. P. Romagnan, and E. Guyon, in *Low Temperature Physics-LT 13: Volume 3: Superconductivity*, edited by K. D. Timmerhaus, W. J. O'Sullivan, and E. F. Hammel (Springer, Boston, MA, 1974), pp. 312–315.

[39] P. Szabó, P. Samuely, J. Kačmarčík, T. Klein, J. Marcus, D. Fruchart, S. Miraglia, C. Marcenat, and A. G. M. Jansen, Phys. Rev. Lett. **87**, 137005 (2001).

[40] R. S. Gonnelli, D. Daghero, G. A. Ummarino, V. A. Stepanov, J. Jun, S. M. Kazakov, and J. Karpinski, Phys. Rev. Lett. **89**, 247004 (2002).

[41] Y. Naidyuk, O. Kvitnitskaya1, D. Bashlakov1, S. Aswartham, I. Morozov, I. Chernyavskii, G. Fuchs, S.-L. Drechsler, R. Hühne, and K. Nielsch, 2D Mater. **5**, 045014 (2018).

[42] Y. Qi, P. G. Naumov, M. N. Ali, C. R. Rajamathi, W. Schnelle, O. Barkalov, M. Hanfland, S.-C. Wu, C. Shekhar, Y. Sun *et al.*, Nat. Commun. **7**, 11038 (2016).

[43] A. A. Tsirlin, P. Fertey, B. R. Ortiz, B. Klis, V. Merkl, M. Dressel, S. D. Wilson, and E. Uykur, arXiv:2105.01397.

[44] Y. G. Naidyuk, G. Fuchs, D. A. Chareev, and A. N. Vasiliev, Phys. Rev. B **93**, 144515 (2016).

[45] S. Medvedev, T. M. McQueen, I. A. Troyan, T. Palasyuk, M. I. Eremets, R. J. Cava, S. Naghavi, F. Casper, V. Ksenofontov, G. Wortmann *et al.*, Nat. Mater. **8**, 630 (2009).

[46] S. Margadonna, Y. Takabayashi, Y. Ohishi, Y. Mizuguchi, Y. Takano, T. Kagayama, T. Nakagawa, M. Takata, and K. Prassides, Phys. Rev. B **80**, 064506 (2009).